Journal of Solid State Chemistry **142,** 206–213 (1999)
Article ID jssc.1998.8036, available online at http://www.idealibrary.com on IDEAL®

Crystal Structures and Electrical and Optical Properties of $MgIn_{2-x}Ga_xO_4$ Solid Solutions

Toshihiro Moriga,[1] Takashi Sakamoto, Yoshiki Sato, Azrul Hisham Khalid @ Haris, Ryoichi Suenari, and Ichiro Nakabayashi

Department of Chemical Science and Technology, Faculty of Engineering, The University of Tokushima, 2-1 Minami-Josanjima, Tokushima 770-8506, Japan

Received April 10, 1998; in revised form September 11, 1998; accepted September 17, 1998

Equilibrium phase relationships in the $MgIn_2O_4$–$MgGa_2O_4$ system at 1400°C were determined by X-ray diffraction. Single phases of the inverse-spinel-type $MgIn_2O_4$, the layered $MgInGaO_4$, and the inverse-spinel-type $MgGa_2O_4$ were observed in a compositional range of $0 \le x \le 0.35$, $0.8 \le x \le 1.0$, and $1.5 \le x \le 2.0$ in $MgIn_{2-x}Ga_xO_4$, respectively. Rietveld structural refinement revealed that the layered $MgInGaO_4$ (space group $R\bar{3}m$, $a = 3.3060(4)$, $c = 25.832(3)$ Å) comprised a InO_2^- single octahedral layer and a $MgGaO_2^+$ double trigonal-bipyramid layer alternatingly stacked along the z-axis. With increasing gallium content, room-temperature conductivity decreased, whereas transparency and optical band gap increased. Results of single-point energy calculation using the CASTEP code supported that $MgIn_2O_4$ is a good conductor with a band gap of ~3.5 eV and that $MgGa_2O_4$ is a poor conductor with a band gap of ~5 eV. © 1999 Academic Press

INTRODUCTION

Transparent conductive oxides (TCOs) are used in a variety of applications including flat panel displays and solar energy conversion devices. The electronic structure of TCOs is scientifically interesting, because metallic conduction behavior is observed even for the materials with optical band gaps greater than 3 eV. ITO (tin-doped indium oxide) is the most important TCO technologically. In addition to ITO, a number of promising TCOs consisting of various oxide combinations of In, Sn and Zn have been reported (1–5). Kawazoe *et al.* have reported that the inverse-spinel-type $MgIn_2O_{4-x}$ is one of the promising new TCOs (6). The spinel-type structure has a three-dimensional network of the rutile chains, connections of edge-shared octahedra, which should play an important role in high electrical conductivity. The optical band gap of $MgIn_2O_{4-x}$ was reported to be 3.4 eV, and the electrical conductivity at room temperature reached almost 10^2 S cm^{-1} with a density of 72% of the theoretical. They have also prepared $MgIn_2O_{4-x}$ thin films by rf-sputtering method and reported that the highest conductivity observed for the films postannealed under H_2 flow was 2.3×10^2 S/cm (7).

Experimental TCOs prepared as $Ga_{2-x}In_xO_3$ with $0 \le x \le 0.85$ are reported to crystallize in the β-gallia-type structure (8). The TCOs improved transparency in green-blue region but the conductivity decreased with increasing Ga content. $MgGa_2O_4$ also has the inverse-spinel-type structure, as does $MgIn_2O_4$. A study on $MgIn_2O_4$–$MgGa_2O_4$ solid–solutions would be interesting in terms of how In and Ga affect electrical and optical properties in the inverse-spinel structure. As nonequilibrium conditions often exist during thin-film deposition, knowledge of equilibrium phase relationships and bulk, physical properties of stable phases can be helpful in interpreting and directing thin-film work. In this paper, we report the synthesis and characterization of TCOs in the $MgIn_2O_4$–$MgGa_2O_4$ system. We also try to explain their properties by employing the computational calculation method.

EXPERIMENTAL

A series of compositions were prepared from basic $MgCO_3$, In_2O_3, and Ga_2O_3 powders (>99.9% purity on cation basis, Kanto Chemicals). The magnesium content of basic $MgCO_3$ was determined by chelatemetry and by thermal gravity analysis, so that the basic $MgCO_3$ was found to have a formula of $4MgCO_3 \cdot Mg(OH)_2 \cdot 5H_2O$. Weighted amounts of the starting powders were ground together with an agate mortar and a pestle. The mixed powder was calcined at 900°C overnight in air and then reground. Pellets (10-mm) uniaxially pressed from this powder at about 100 MPa were heated in covered alumina crucible at 1400°C for 48 h and subsequently quenched in air by pulling them out of the furnace using stainless tongs. To minimize contamination from the alumina crucible and to inhibit vaporization of In_2O_3 during firing, each pellets

[1]To whom correspondence should be addressed.

0022-4596/99 $30.00
Copyright © 1999 by Academic Press
All rights of reproduction in any form reserved.

were surrounded by their constituent powders. The phase identification and the lattice parameter determination were performed by powder X-ray diffraction (Rigaku RINT2500VHF$^+$, Japan) using Cu$K\alpha$ radiation with a source power of 40 kV and 150 mA. Lattice parameters were calculated with a least-square averaging program.

The structure refinement was carried out by X-ray Rietveld analysis with the RIETAN94 program (9). Diffraction data were collected by step scanning over the angular range of $20^\circ \le 2\theta \le 100^\circ$ in increments of 0.04° in 2θ. The fixed time for each point was 2 s. The refinement was done in stage, with the atomic coordination and thermal parameters held fixed in initial calculations and subsequently allowed to vary after scale, background, peak-shape, and lattice parameters were close to convergence to their optimum values. The preferred orientations of the sample (March–Dollase function) were taken into account.

Electrical conductivity and diffuse reflectance of sintered pellets were measured before and after reducing in a diluted H_2 gas ($10H_2$–$90\%N_2$) at 500°C for 1 h. The pellets were furnace-cooled after the reduction in a stream of the H_2 gas. Room-temperature electrical conductivity of the samples was measured with a spring-loaded linear four-probe apparatus (YTS, Tokushima, Japan) using a current source and voltmeter (Models R6144 and R6551, Advantest, Japan). Excitation currents were 1–10 mA. The conductivity was calculated as

$$\sigma = \frac{1}{\rho} = \frac{1}{\frac{V}{I} wC\left(\frac{d}{s}\right) F\left(\frac{w}{s}\right)},$$

where σ is conductivity, ρ is resistivity, V is measure voltage, I is excitation current, w is width, d is diameter, s is electrode spacing, and $C(d/s)$ and $F(w/s)$ are correction factors for sample geometry and finite thickness, respectively (10). The pellets used for these tests had relative densities from 50 to 60% of theoretical. To account for variation in the densities among the measured samples, conductivity values were divided by the relative density of the corresponding sample. Diffuse reflectance was measured from 200 to 800 using a spectrophotometer with integrating sphere (JASCO V-550DS, Japan). A scan rate of 500 nm/min, a data interval of 1.0, and a signal averaging time of 0.1 s was applied. A blackened sample mask was used to mount pellet sample. Measurements were made in reference to PTFE compact.

The single-point energy calculations for $MgIn_2O_4$ and $MgGa_2O_4$ were performed using the CASTEP (Cambridge Serial Total Energy Package) code, installed as one of the application programs that make up the Cerius^2 3.0 (Moleculer Simulation Inc.). Generalized gradient approximations (GGA) were chosen for the theoretical basis of density function (11, 12). The code used the band-by-band conjugate-gradient technique to minimize the total energy with respect to plane-wave expansion coefficient (13, 14). Lattice parameters and atomic coordinates were fixed at the values obtained by the X-ray Rietveld analysis. As both $MgIn_2O_4$ and $MgGa_2O_4$, however, take the inverse-spinel-type structure, half of the In occupies the 8(a) site and Mg and the other half of In (or Ga) occupies the 16(d) site in the space group of $Fd\bar{3}m$ statistically. So Mg and In (or Ga) should be visually distributed over the 16(d) site in the calculation models, as shown in Fig. 1. In setting up the CASTEP run, basic parameters were chosen as follows: 56 atoms (8 magnesiums, 16 indiums (or 16 galliums), and 32 oxygens in a unit cell), kinetic energy cutoff = 330 eV, k-point spacing = 0.05 Å^{-1}, sets of k-points = $3 \times 3 \times 3$, fast Fourier transform (FFT) grid dimensions = $40 \times 40 \times 40$, and space representation = reciprocal.

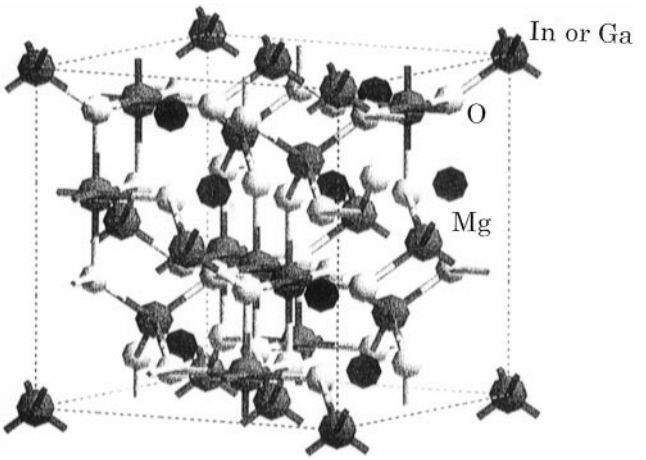

FIG. 1. Structural model of $MgIn_2O_4$ (or $MgGa_2O_4$) for the single-energy calculation. Black, gray, and white spheres represent Mg, In or Ga, and O, respectively.

RESULTS AND DISCUSSION

Figure 2 shows variation of X-ray diffraction pattern of $MgIn_{2-x}Ga_xO_4$. A single phase of the inverse-spinel-type $MgIn_2O_4$ was observed in a compositional range of $0 \le x \le 0.35$, and that of the inverse-spinel-type $MgGa_2O_4$ was observed in a range of $1.5 \le x \le 2.0$. However, several new diffraction lines, which could not be indexed as both the inverse-spinel phases, appeared in a range of $0.4 \le x \le 1.5$. In a range of $0.8 \le x \le 1.0$, only these new lines could be observed. As a result of searching JCPDS cards, this new phase could be considered to be isostructural to $MgInGaO_4$ (No. 38-1106) and $InGaZnO_4$ (No. 38-1104). The ideal stoichiometric composition of this phase would be $MgInGaO_4$. The rhombohedral $MgInGaO_4$ phase was independently identified in the course of studies on the In_2O_3–A_2O_3–BO systems (A = Fe, Ga, Al; B = Mg, Mn, Fe, Ni, Co, Cu, Zn) by Kimizuka *et al.* (15, 16). Lattice

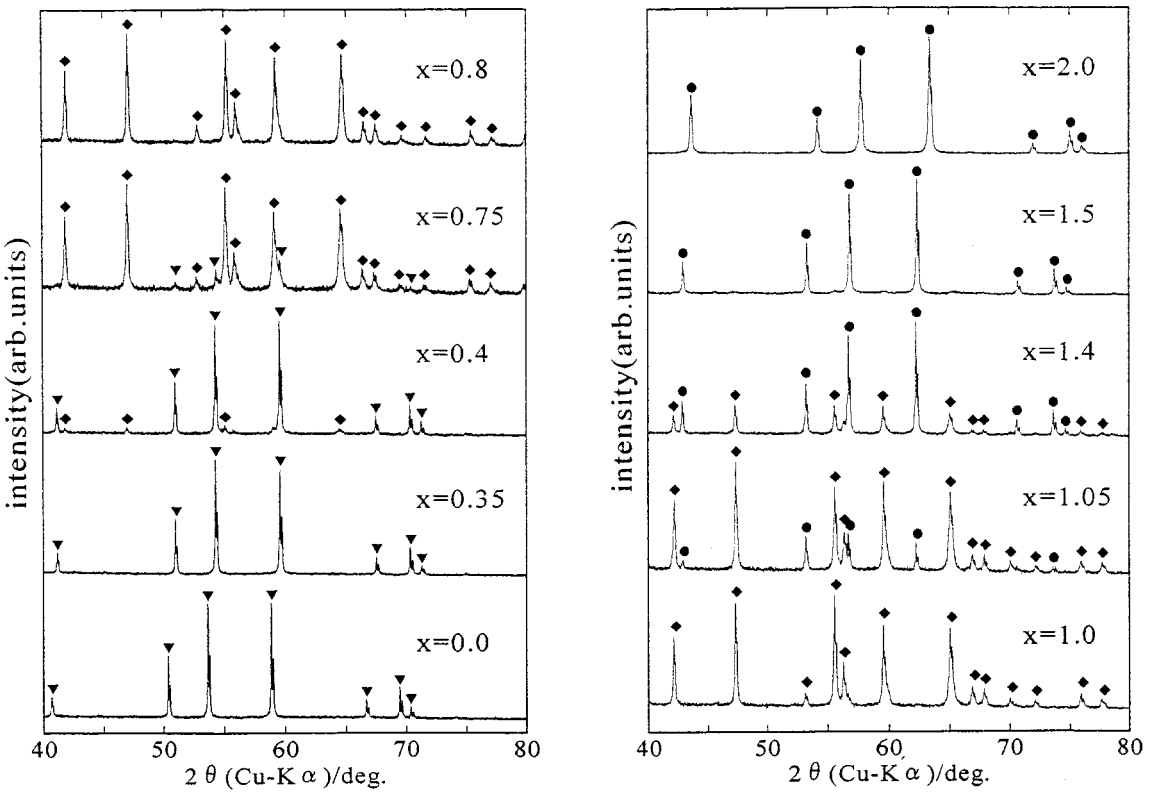

FIG. 2. Variation of X-ray diffraction patterns of $MgIn_{2-x}Ga_xO_4$. Diffraction peaks with triangles, diamonds, and circles are assigned to the cubic $MgIn_2O_4$-, the rhombohedral $MgInGaO_4$-, and the $MgGa_2O_4$-phases, respectively.

parameters were calculated using the d values of (10$\underline{1}$0), (110), (10-$\underline{14}$), and (119) reflections for the rhombohedral $MgInGaO_4$-phase and those of (400), (511), and (440) reflections for the cubic inverse-spinel phases, respectively. The result for samples in single-phase region is shown in Table 1. The lattice parameters obtained for $MgInGaO_4$ (a = 3.3054(2) Å and c = 25.833(4) Å) are slightly larger than those reported by Kimizuka and Mohri (a = 3.3036(1) Å and c = 25.805(1) Å) (16). However, the lattice parameters for $MgIn_{1.2}Ga_{0.8}O_4$ (a = 3.3252(4) Å and c = 25.962(7) Å) are in a good agreement with those reported by Barbier (a = 3.3243(4) Å and c = 25.954(3) Å) (17), respectively. These results may be attributable to the difference of firing temperatures. Samples were fired at 1300°C in Kimizuka's work and at 1400°C in Barbier's and our works. Substitution of In cation by the smaller Ga cation in both the three phases resulted in a decrease in the cell volume, as illustrated in Fig. 3. The cell volume was divided by the number of formula units per unit cell (z); i.e., $z = 3$ for the rhombohedral $MgInGaO_4$ phase and $z = 8$ for the cubic

TABLE 1
Some Crystallographic Data Obtained by the Rietveld Refinement of $MgInGaO_4$

Space group		$R\bar{3}m$			
Scale factor	s	0.000269(2)	Lattice constant	a/Å	3.3060(4)
Gaussian FWHM parameter	U	0.00259(4)		c/Å	25.832(3)
	V	0.00463(4)			
	W	−0.000280(7)	Reliability factor	R_{wp}	12.31
Lorentzian Scherrer broadening	X	0.0164(9)		R_p	8.92
Anisotropic Scherrer broadening	Xe	−3.56(10)		R_R	10.86
Strain broadening	Y	0.157(3)		R_E	6.10
Anisotropic strain broadening	Ye	0.071(3)		R_I	3.36
Asymmetry parameter	As	0.0864(2)		R_F	1.91
Preferred-orientation parameter	r	0.933(4)			

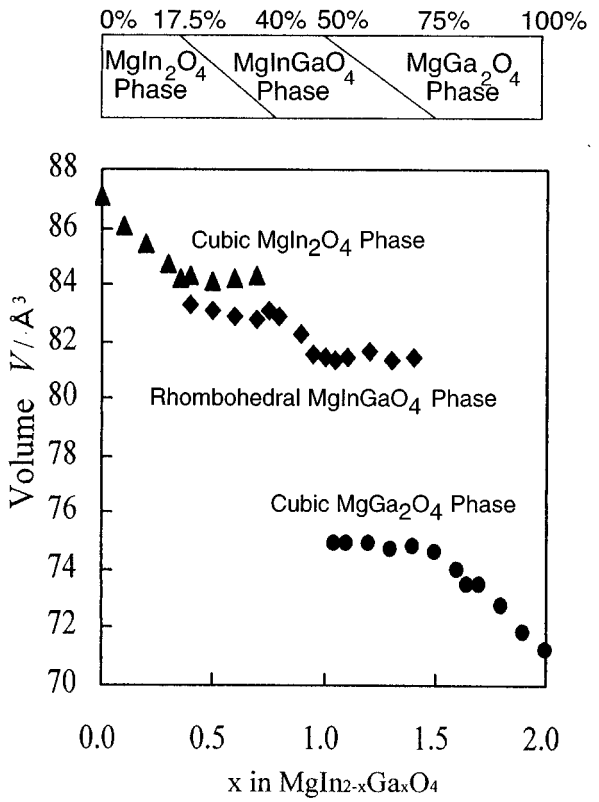

FIG. 3. Cell volume of $MgIn_{2-x}Ga_xO_4$ as a function of x.

inverse-spinel phases, respectively. In a single-phase region of the respective phases, the volume decreased linearly with increasing gallium content. It seemed that $MgInGaO_4$ phase is sparser than the other inverse-spinel phases.

TABLE 2
Positional and Thermal Parameters of $MgInGaO_4$

Atom	Position[a]	x	y	z	B/Å
In	3(a)	0	0	0	0.9(3)
$Mg_{0.5}Ga_{0.5}$	6(c)	0	0	0.2168(4)	0.3(3)
O(1)	6(c)	0	0	0.1282(10)	1.3(9)
O(2)	6(c)	0	0	0.2922(14)	0.8(8)

[a] Multiplicity and Wyckoff notation.

Rietveld analyses for the compounds of $MgIn_2O_4$ and $MgGa_2O_4$ supported that both the compounds have the inverse-spinel-type structure (space group; $Fd\bar{3}m$; lattice parameter and positional parameter x at 32(e) site, $a = 8.864(5)$ Å, $x = 0.386(6)$ for $MgIn_2O_4$; and $a = 8.292(5)$ Å, $x = 0.377(6)$ for $MgGa_2O_4$, respectively). Rietveld analysis for $MgInGaO_4$ was carried out in reference to the positional parameters of $MgIn_{1.2}Ga_{0.8}O_4$ (17) and $LuFeO_3 \cdot ZnO$ (18), in which In occupies the 3(a) site, Mg and Ga statistically occupy the 6(c) site. A space group of $R\bar{3}m$ (hexagonal setting) was assumed. The observed, calculated, and difference plots of the result in the Rietveld analysis of $MgInGaO_4$ are shown in Fig. 4. The result of the analysis is shown in Tables 2 and 3, and schematic representation of the structure of $MgInGaO_4$ is shown in Fig. 5. The basic structure consists of InO_2^- and $MgGaO_2^+$ layers alternatively stacked along the z-axis. Edge-shared InO_6 octahedra form a continuous layer on the c-plane. The Mg or Ga at the 6(c) site shift from the center of gravity of the tetrahedra along the opposite direction to the apical

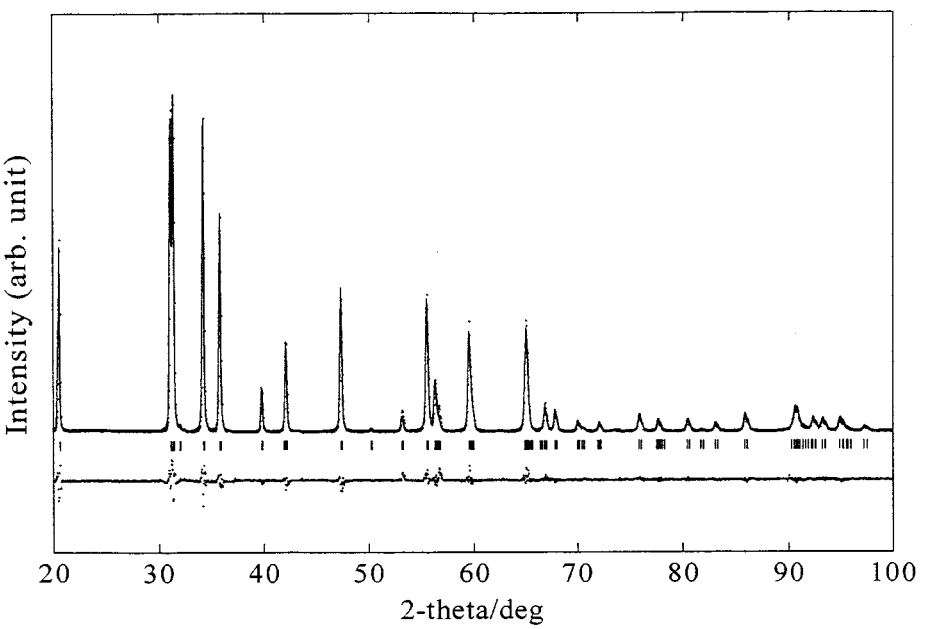

FIG. 4. Observed, calculated and difference plots of the result in Rietveld analysis of $MgInGaO_4$.

TABLE 3
Lattice Parameters for $MgIn_{2-x}Ga_xO_4$

x^a	$MgIn_2O_4$ phases a (Å)	$MgInGaO_4$ phase a (Å)	$MgInGaO_4$ phase c (Å)	$MgGa_2O_4$ phase a (Å)
0.00	8.864(5)			
0.10	8.829(9)			
0.20	8.809(7)			
0.30	8.786(4)			
0.35	8.765(4)			
0.80		3.3252(4)	25.962(7)	
0.90		3.3164(9)	25.910(20)	
0.95		3.3080(4)	25.825(7)	
1.00		3.3054(2)	25.833(4)	
1.50				8.418(2)
1.60				8.396(6)
1.65				8.380(20)
1.70				8.371(7)
1.80				8.348(5)
1.90				8.315(8)
2.00				8.292(5)

[a] x in $MgIn_{2-x}Ga_xO_4$.

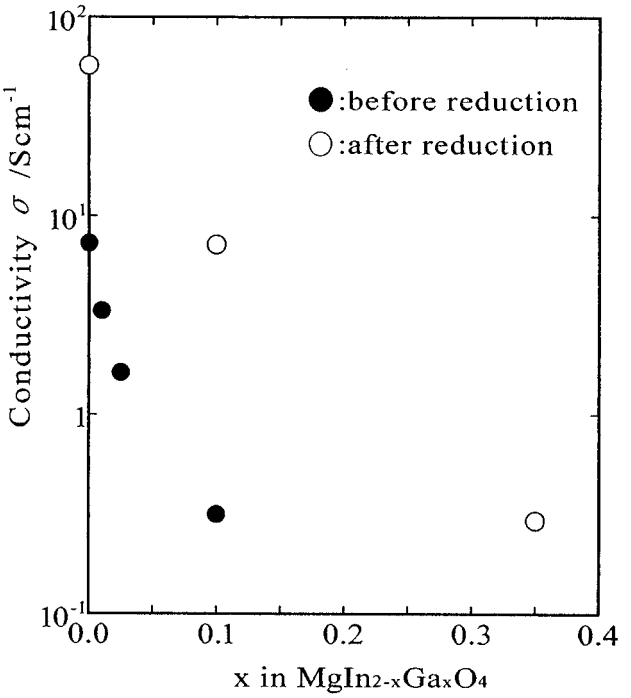

FIG. 6. Variation of electrical conductivity of $MgIn_{2-x}Ga_xO_4$ as a function of x.

oxygen to form a trigonal bipyramid. From the results of Rietveld analysis for several samples with the $MgInGaO_4$-type phase, gallium cation did not occupy the octahedral 3(*a*) indium site, resulting in phase separation into $MgInGaO_4$-type and $MgGa_2O_4$-type phases in a compositional range above $x > 1.0$. Barbier also emphasized that $MgIn_{1.2}Ga_{0.8}O_4$ contains indium at the 3(*a*) site and indium, gallium, and magnesium disorderly at the 6(*c*) site (17).

Figure 6 shows electrical conductivity versus gallium content in $MgIn_{2-x}Ga_xO_4$ for samples with the $MgIn_2O_4$ phase. Conductivities for samples with the $MgInGaO_4$ and the $MgGa_2O_4$ phases were too low to be measured. Considering the instrument off-scale set-point, their conductivities were estimated be less than 10^{-3} S cm^{-1}. The conductivity of the $MgIn_{2-x}Ga_xO_4$ decreased with increasing gallium content. Reduction in the 10% H_2 gas resulted in increased conductivity for the solid solutions, presumably because of the formation of oxygen vacancies which serve as electron donors. The conductivity of $MgIn_2O_4$ increased by almost one order of magnitude upon the reduction to be 70 S cm^{-1}. The effect of reduction on the resulting conductivity seemed to increase with increasing gallium content.

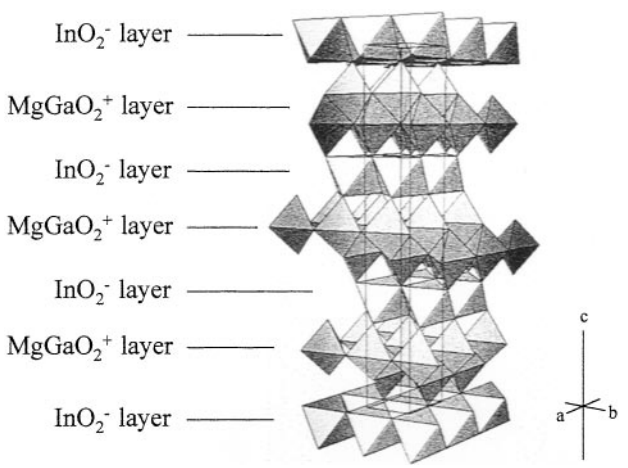

FIG. 5. Schematic representation of structure of $MgInGaO_4$.

The color of the quenched samples ranged from light gray-blue (low gallium content) to white (high gallium content). Figure 7 shows variation of the diffuse reflectance spectrum of $MgIn_{2-x}Ga_xO_4$. Diffuse reflectance spectra of bulk sample are analogous to transmission spectra of thin sample (20). The fundamental absorption edge of $MgIn_2O_4$ ($x = 0.0$) was around 360 nm, suggesting a band gap near 3.45 eV. The absorption edge shifted to the shorter wavelength with increasing gallium content, reaching to around 245 nm (4.95 eV). The transmittance (reflectance) at $\lambda > 400$ nm of all the samples was higher than that of ITO (3% Sn, $\lambda_{\text{abs-edge}} \simeq 400$ nm, $R_{\lambda=500\,\text{nm}} = 40\%$) and increased with gallium content. Pellet colors of samples with the $MgIn_2O_4$ phase grew darker visibly after reduction in the 10% H_2 gas. Concerning the $MgIn_2O_4$ sample, though the onset position of absorption

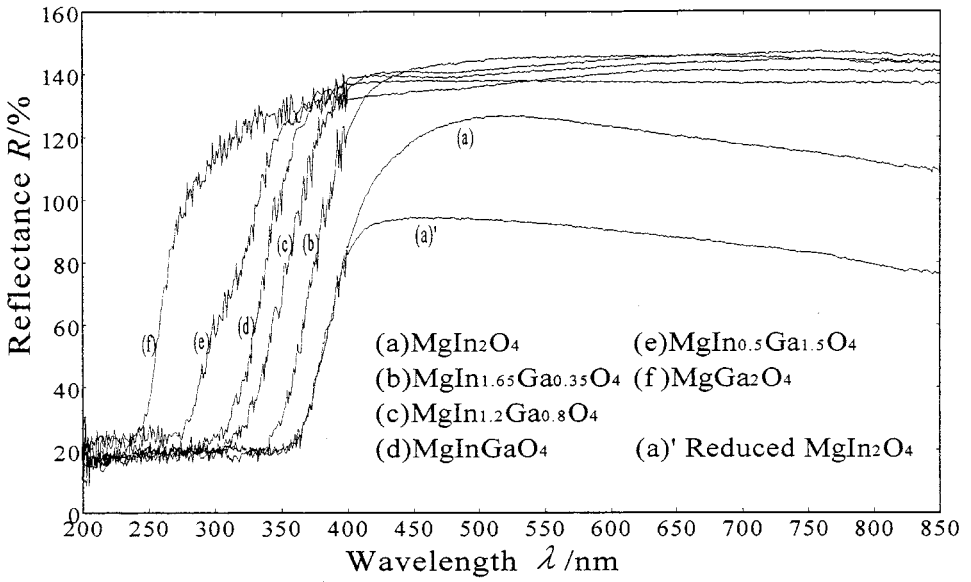

FIG. 7. Variation of diffuse reflectance spectra of $MgIn_{2-x}Ga_xO_4$ as a function of x.

edge was unchanged, transmittance at $\lambda > 400$ nm lowered by the order of $\sim 30\%$ through the reduction. This would be due to an increase of carrier concentration (21). This phenomenon was also observed for the other samples, not shown in Fig. 7.

From the results of Rietveld analysis for $MgIn_2O_4$ and $MgGa_2O_4$, the u-parameter, which is same as the positional parameter x of the 32(e) site (the ideal value of the u parameter is 0.375), was found to be 0.386(6) for $MgIn_2O_4$ and 0.377(6) for $MgGa_2O_4$. The observed distance between

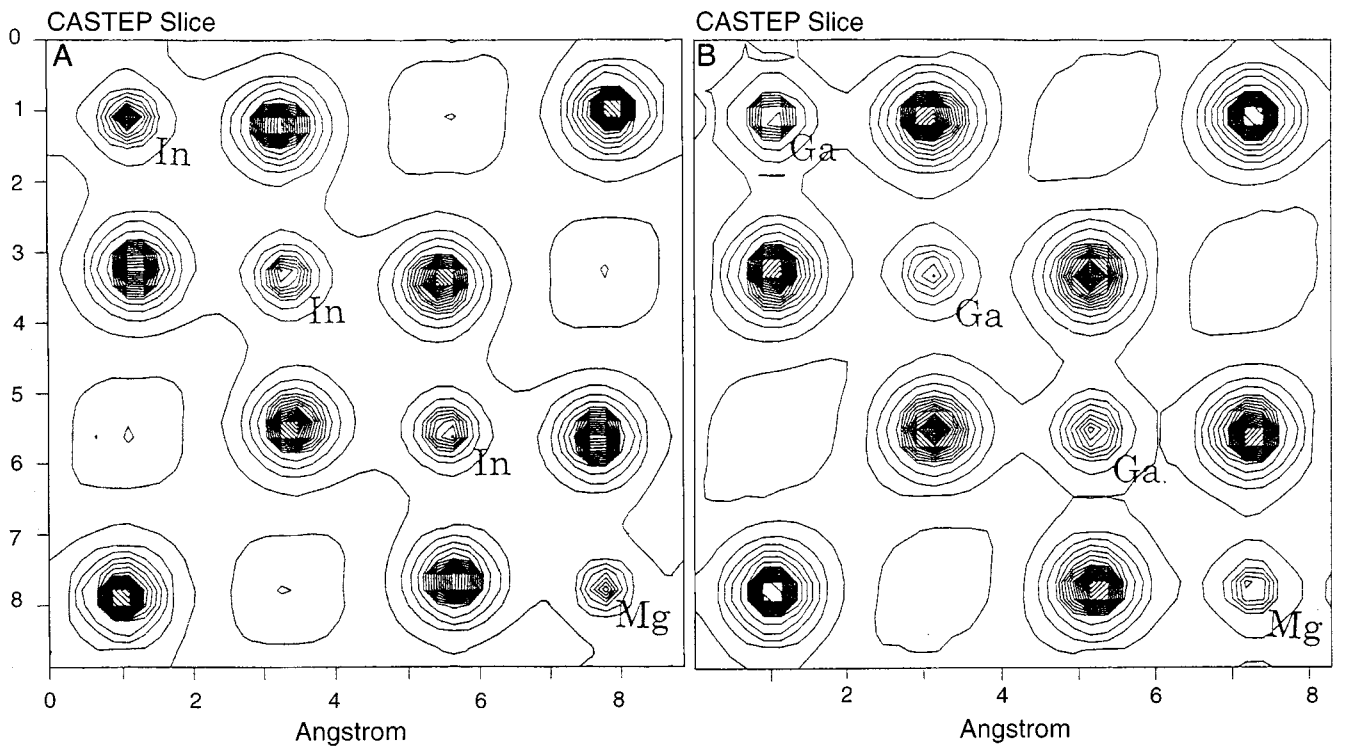

FIG. 8. Electrostatic potential contours at $z = 3/8$ in the (0 0 1) plane for (A) $MgIn_2O_4$ and (B) $MgGa_2O_4$. Sites which are not denoted are occupied by oxygens.

16(d) metal site and 32(e) oxygen site in the octahedron can be calculated according to

$$d = a\left(\frac{5}{8} - u\right),$$

where d is the distance, a is lattice parameter, and u is u-parameter, respectively (22). Using this formula, the distance is calculated to be 2.12(1) Å for $MgIn_2O_4$ and 2.06(1) Å for $MgGa_2O_4$, respectively. The expected distance can be calculated by the sum of effective ionic radius of the corresponding species (23). As both $MgIn_2O_4$ and $MgGa_2O_4$ take the inverse-spinel-type structure, the 16(d) site is occupied by half indiums (or galliums) and half magnesiums. The sums of sixfold In^{3+} and the fourfold O^{2-}, sixfold Ga^{3+}, and the fourfold O^{2-} and sixfold Mg^{2+} and the fourfold O^{2-} are 2.18, 2.00, and 2.10 Å, respectively. The expected distance is, therefore, 2.14 Å for $MgIn_2O_4$ and 2.05 Å for $MgGa_2O_4$. The observed and expected values agree well. It might be expected that the substitution of Ga for In should not give any carriers. These facts mean that it is not the structural factors but the nature of the constituent species that affect the difference in physical properties.

Figures 8A and 8B show electrostatic potential contours at $z = 3/8$ in the (001) plane (cf. Fig. 1) for $MgIn_2O_4$ and $MgGa_2O_4$ obtained by the single-point energy calculation, which enables us to evaluate the potential energy and other ground state properties of the given structure. In these figures, the rutile chain runs along the face-diagonal axis, from bottom right to top left. Three indiums (or galliums) and one magnesium are arranged in this order. In Fig. 8A, the continuous band was formed along the rutile chain so that electrons can easily move through the chain. On the contrary, several nodes breaking the band off appeared across the rutile chain in Fig. 8B. We can imagine that $MgGa_2O_4$ would be a poorer electron conductor than $MgIn_2O_4$. It can be considered that the substitution of Ga for In in the $MgIn_{2-x}Ga_xO_4$ system would break the conduction paths along the rutile chains, resulting in the decrease in electrical conductivity. The densities of state (DOS) for these compounds were also calculated, one of which, for $MgIn_2O_4$, is shown in Fig. 9. The energy as abscissa was not corrected in reference to the Fermi level. The valence band just below the Fermi level (so-called HOMO) was mainly composed of O2p and the conduction band just above the Fermi level (LUMO) was mainly composed of In5s, 5p. The band gap for $MgIn_2O_4$ was 3.64 eV. As for $MgGa_2O_4$, the band gap was 4.55 eV, calculated from the chart of DOS. These values are in a good agreement with the experimental value estimated from the diffuse reflectance spectra. It has been reported that In_2O_3 has a band gap of 3.7 eV (24) and the O2p and the In5s makes up of the HOMO and the LUMO (25), respectively, and that β-Ga_2O_3 has a band gap of 4.8 eV (26). The physical properties resulting from the electronic structure for $MgIn_2O_4$ and $MgGa_2O_4$ should reflect those for In_2O_3 and β-Ga_2O_3, respectively.

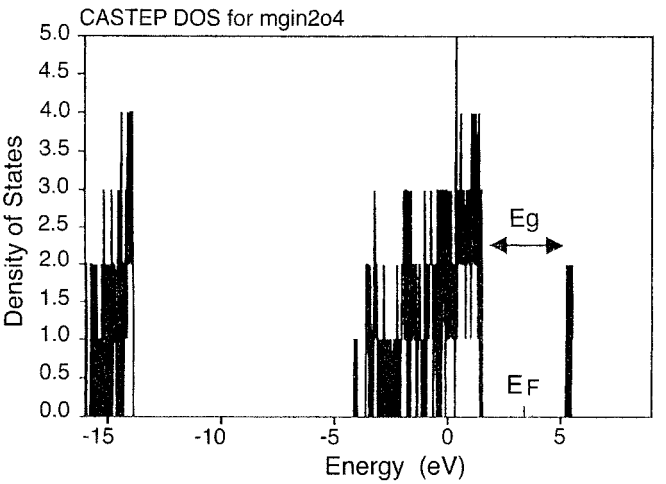

FIG. 9. Density of states for $MgIn_2O_4$. Fermi level and band gap are shown in the figure.

ACKNOWLEDGMENT

This work was partly supported by a Grant-in-Aid for Scientific Research form the Ministry of Education, Science, and Culture.

REFERENCES

1. J. M. Phillips, R. J. Cava, G. A. Thomas, S. A. Carter, J. Kwo, T. Siegrist, J. Krajewski, J. Marshall, W. Peck, and D. Rapkine, *Appl. Phys. Lett*. **67,** 2246 (1995).
2. R. Wang, A. Sleight, R. Platzer, and J. A. Gardner, *J. Mater. Res.* **11,** 1659 (1996).
3. D. D. Edwards, T. O. Mason, F. Goutenoire, and K. R. Poeppelmeier, *Appl. Phys. Lett*. **70,** 1706 (1997).
4. G. B. Palmer, K. R. Poeppelmeier, and T. O. Mason, *Chem. Mater*. **9,** 3121 (1997).
5. T. Moriga, D. D. Edwards, T. O. Mason, G. B. Palmer, K. R. Poeppelmeier, J. L. Schindler, C. R. Kannewarf, and I. Nakabayashi, *J. Am. Ceram. Soc*. **81,** 1310 (1998).
6. N. Ueda, T. Omata, N. Kazushige, H. Mizoguchi, T. Hashimoto, and H. Kawazoe, *Appl. Phys. Lett*. **61,** 1954 (1992).
7. H. Un'no, N. Hikuma, T. Omata, N. Ueda, T. Hashimoto, and H. Kawazoe, *Jpn. J. Appl. Phys.* **32,** L1260 (1993).
8. D. D. Edwards, P. E. Folkins, and T. O. Mason, *J. Am. Ceram. Soc.* **80,** 253 (1997).
9. F. Izumi, *in* "The Rietveld Method" (R. A. Young, Ed.), pp. 236–253, Oxford Univ. Press, London, 1993.
10. F. M. Smits, *Bell Syst. Tech. J*. **37,** 711 (1958).
11. J. P. Perdew and Y. Wand, *Phys. Rev. B* **46,** 6671 (1992).
12. J. A. White and D. M. Bird, *Phys. Rev. B* **50,** 4954 (1994).
13. J. Gillan, *J. Phys. Cond. Matter* **1,** 689 (1989).
14. M. C. Payne, M. P. Teter, D. C. Allan, T. A. Arias, and J. D. Joannopoulos, *Rev. Mod. Phys.* **64,** 1045 (1992).

15. N. Kimizuka and E. Takayama, *J. Solid State Chem.* **53,** 217 (1984).
16. N. Kimizuka and T. Mohri, *J. Solid State Chem.* **60,** 382 (1985).
17. J. Barbier, *J. Solid State Chem.* **82,** 115 (1989).
18. M. Isobe, N. Kimizuka, M. Nakamura, and T. Mohri, *Acta Crystallogr. C* **50,** 332 (1994).
19. H. G. Hecht, *in* "Modern Aspects of Reflectance Spectroscopy" (W. W. Wendlandt, Ed.) pp. 1–26. Plenum, New York, 1968.
20. I. Hamberg and C. G. Granqvist, *J. Appl. Phys.* **60,** R123 (1986).
21. B. G. Hyde and S. Andersson, "Inorganic Crystal Structures," pp. 37–39. Wiley, New York, 1989.
22. R. D. Shannon, *Acta Crystallogr. A* **32,** 751 (1976).
23. Z. M. Jarzebski, *Phys. Status Solidi A* **71,** 13 (1982).
24. M. Mizuno, I. Tanaka, and H. Adachi, *Bull. Soc. DV-Xα*, **10,** 92 (1997).
25. N. Ueda, H. Hosono, R. Waseda, and H. Kawazoe, *Appl. Phys. Lett.* **71,** 933 (1997).